Origin of strong white electroluminescence from dense Si nanodots embedded in silicon nitride

R. Huang,[1,5] J. Song,[1] X. Wang,[1] Y. Q. Guo,[1] C. Song,[1] Z. H. Zheng,[1] X. L. Wu,[2,4] and Paul K. Chu[3,6]

[1]*Department of Physics and Electrical Engineering, Hanshan Normal University, Chaozhou, Guangdong, 521041, China*

[2]*State Key Laboratory of Solid State Microstructures and Department of Physics, Nanjing University, Nanjing 210093, China*

[3]*Department of Physics and Materials Science, City University of Hong Kong, Tat Chee Avenue, Kowloon, Hong Kong, China*

[4]*e-mail: hkxlwu@nju.edu.cn*

[5]*e-mail: rhuang@hstc.edu.cn*

[6]*e-mail: paul.chu@cityu.edu.hk*

Received November 15, 2011; revised December 9, 2011; accepted December 15, 2011; posted December 19, 2011 (Doc. ID 158189); published February 14, 2012

Strong white electroluminescence (EL) from SiN-based devices containing Si nanodots with a density of more than $4.6 \times 10^{12}/\mathrm{cm}^2$ was investigated. The white EL illustrates enhanced light emission with increasing applied voltage and can be divided into two components, a dominant peak at ~710 nm and weak one at ~550 nm, which are close to those of the PL spectra optically pumped by the 325 and 488 nm lines, respectively. Based on the PL characteristics, we propose that the dominant EL band arises from the band-to-band recombination in the dense Si nanodots where quantum confinement plays a decisive role in the light emission, whereas the weak EL band originates from the radiative Si dangling bond (K^0) centers in the silicon nitride matrix.

OCIS codes: 160.4236, 230.3670, 260.3800.

Silicon nanomaterials have been studied extensively for potential applications in efficient Si-based light sources to realize monolithic optoelectronic integrated circuits [1–4]. Since electron–hole interactions can be accentuated in low-dimensional structures, much effort has been made to fabricate dense Si nanostructures with good surface passivation so as to accomplish efficient luminescence [5–7]. Although some progress has been made, the efficiency of electroluminescence (EL) from this system is still quite low [2,8–11]. Photoluminescence (PL) is an instant excitation and recombination process, whereas EL involves radiative recombination of electrically excited carriers and passage of injected electrons and holes through the host matrix. Hence, the host matrix is crucial to the EL efficiency. In recent years, silicon nitride has been proposed to be an alternative host matrix to achieve effective EL at a low driving voltage because of its relatively low barrier to electrons and holes compared to silicon oxide [12–15]. However, silicon nitride generally contains various defect centers such as Si and N dangling bonds, which can act as radiative EL centers to give rise to light emission in the yellow to violet region [15,16]. This complicates the EL properties of the silicon nanostructure/silicon nitride systems and more importantly, the luminescence properties of the Si nanostructures can degrade since these defects have radiative lifetimes on the order of nanoseconds and they are much shorter than those of Si nanostructures [2,17]. Although recent studies have explored efficient EL from the silicon nitride system, the progress so far is slow [12–16,18]. In particular, studies on EL from dense Si nanostructures have been relatively rare [9,12] and the mechanism responsible for the EL origin is still unclear.

In this Letter, we report bright white EL from SiN-based devices that contain Si nanodots with a density of over $4.6 \times 10^{12}/\mathrm{cm}^2$. The white EL consists of two components with the dominant peak at ~710 nm and the weaker one at ~550 nm. By examining the PL characteristics, we propose that the dominant EL band arises from the band-to-band recombination in the dense Si nanodots and the weak EL band originates from radiative Si dangling bond (K^0) centers in the silicon nitride matrix.

Amorphous SiN_x (a-SiN_x) film containing Si nanodots was deposited on indium tin oxide (50 Ω/□) on glass and used as a luminescent active layer in the current light-emitting device. The luminescent active layer with a thickness of 30 nm was prepared from silane diluted with ammonia and hydrogen in a conventional parallel plate radiofrequency (40.68 MHz) glow discharge system. The flow rates of SiH_4, NH_3, and H_2 were 10, 50 and 90 sccm, respectively. A power density of 0.6 $\mathrm{W/cm}^2$ was used in the experiments and the process was conducted at a relatively low temperature of 250 °C. The pressure in the chamber was kept at 60 Pa. To fabricate the light-emitting device, an Al thin film was evaporated onto the surface as the cathode. The current density-voltage (J-V) characteristics of the device were measured under forward-biasing conditions at room temperature using a KEITHEY-2611A source meter. The PL measurements were carried out at room temperature using an Ar^+ laser (488 nm) or He–Cd laser (325 nm) as the excitation source. The EL spectra were acquired on a Fluorolog-3 fluorescence spectrophotometer and the structure of the Si nanodots was determined by transmission electron microscopy (TEM) on the JEM-4000EX microscope.

Figure 1(a) shows the EL emission from the device operated at different electrically excited levels under forward biasing. The EL emission peak at ~740 nm can be detected when the forward bias (V_{bias}) is only at 4 V. The EL spectrum shows enhanced light emission from red to white with increasing applied voltages due to the increase of the high-energy luminescence. At a V_{bias} of

11.5 V, the strong uniform white emission has a linewidth of ~280 nm and is visible under room light, as shown in the inset of Fig. 1(b). The broad EL band can be divided into two Gaussian profiles. The one on the low energy side corresponds to the dominant EL band at ~710 nm, whereas the other one on the higher energy side is related to the weak EL band at ~550 nm, as shown in Fig. 1(b). The dominant EL emission is different from that observed by Chen *et al.* who observed that the dominant EL peak was at 443 nm (2.8 eV) [12]. To determine the origin of the strong white EL, the microstructure of the SiN luminescent active layer was characterized by TEM. The cross-sectional TEM image [Fig. 1(c)] reveals the presence of Si nanodots as well-separated dark spots on a bright background homogeneously distributed throughout the SiN_x active layer. The dot density is estimated to be $\sim 4.6 \times 10^{12}/\mathrm{cm}^2$. The dot size ranges from 1.2 to 6.0 nm exhibiting a Lorentzian-like distribution as indicated in Fig. 1(d). The mean size is about 2.4 nm. The Raman peak at ~480 cm^{-1} [inset in Fig. 1(d)] resembles the typical feature of a-Si vibration mode. According to Fig. 1(c), the high density of a-Si nanodots appears to be responsible for the strong white emission.

The origins of the white EL emission are further investigated by comparing the EL and PL spectra of the devices. Figures 2(a) and 2(b) show the PL spectra acquired from the luminescent active layer sample at different excitation wavelengths and temperature. When excited by the 325 nm line, a PL peak at ~550 nm emerges, but when excited by the 488 nm line, a red emission band centered at 650–685 nm can be observed. The positions of the two emission peaks taken under the 325 and 488 nm lines

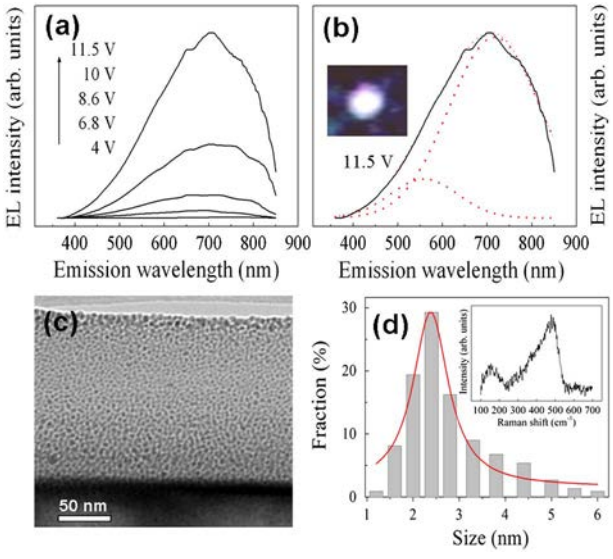

Fig. 1. (Color online) (a) Room temperature EL spectra of the device measured under the following biases with current densities: (1) 4.0 V and 12 $\mathrm{mA/cm}^2$, (2) 6.8 V and 58 $\mathrm{mA/cm}^2$, (3) 8.6 V and 130 $\mathrm{mA/cm}^2$, (4) 10 V and 264 $\mathrm{mA/cm}^2$, (5) 11.5 V and 452 $\mathrm{mA/cm}^2$. (b) White EL band can be devoluted into two Gaussian profiles at ~550 and ~710 nm, respectively. The inset shows the photograph of the emitted light. (c) Bright-field cross-sectional TEM image of the Si nanodots in the SiN_x sample. (d) Size distribution as extracted from the TEM image for Si nanodots. The inset shows the Raman spectrum obtained from the sample.

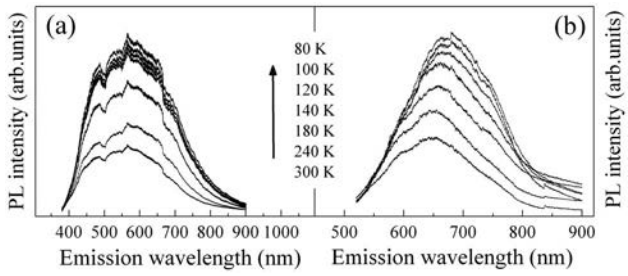

Fig. 2. PL spectra at different temperatures excited by the (a) 325 nm line and the (b) 488 nm line.

are very close to those of the decomposed EL spectrum [Fig. 1(b)]. This results indicate that both the PL emission excited by the 488 nm line and dominant EL emission have the same origin and the PL emission excited by the 325 nm line corresponds to the weak EL emission on the high-energy side. As shown in Fig. 2(a), one can also see that the position of the PL peak excited by the 325 nm line is independent of the temperature. This indicates that the 550 nm PL emission may be due to radiative recombination via interface states or luminescent centers existing in the a-SiN_x host matrix instead of band-to-band recombination in the Si nanodots. With regard to the a-Si nanodots embedded in the SiN_x matrix, since the N atoms bonded to the surface of Si nanodot would result in a broad near-IR emission [5], it can be inferred that the 550 nm PL emission is not from the surface state of radiative recombination but rather the SiN_x matrix. According to Robertson and Powell [19], it is believed that the 550 nm PL emission arises from radiative recombination at Si dangling bonds (K^0). Concerning the red light emission excited by the 488 nm line, if the quantum confinement mechanism governs the PL process, the energy gap (E) of a-Si quantum dots can be expressed as $E(\mathrm{eV}) = 1.56 + 2.4/d^2$ according to the effective mass theory [5], where d is the quantum dot size. Accordingly, the energy gap of nanodots with a mean size of 2.4 nm is estimated to be 1.97 eV, which is close to the red light emission (1.91 eV) observed from the corresponding samples, indicating that the red light emission arises from band-to-band recombination in the a-Si nanodots. Therefore, it can be understood that the slight PL redshift with decreasing temperature is due to the enhanced radiative

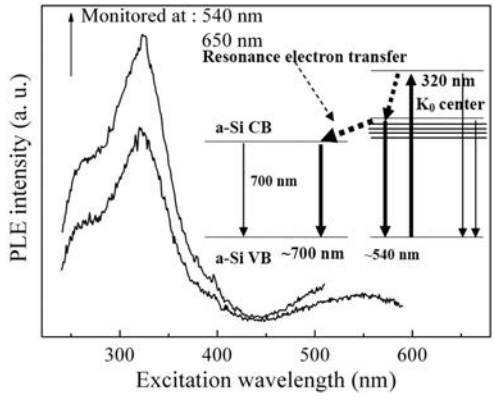

Fig. 3. PLE spectra monitored at 550 and 650 nm. The inset shows the energy level schematic diagrams of the excitation, transfer, and recombination processes of electrons.

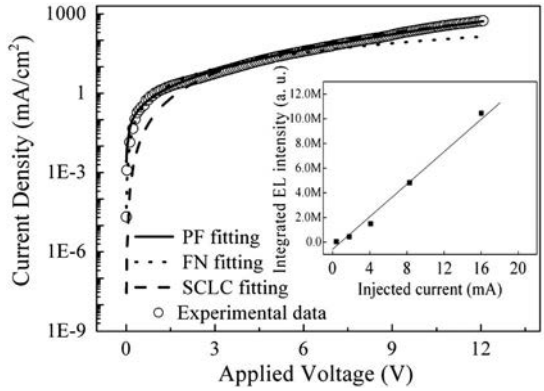

Fig. 4. Current density-voltage (J-V) characteristics of the devices under forward biasing with the experimental data fitted by $J = C_1V \exp(B_1V^{1/2})$) for PF emission (solid), $J = C_2V^m$ for SCLC (dash), and $J = C_3V^2 \exp(-B_2/V)$ for FN tunneling (dot) [13–14]. The inset shows the plots of the integrated EL intensity as a function of injection current for the device.

recombination probability of electron–hole pairs in larger Si nanodots at low temperatures [20]. To explore the photoexcited process of carriers, the PLE spectra monitored at 550 and 650 nm are shown in Fig. 3. The resonance excitation peak at around 320 nm in both the PLE spectra is clearly observed. In addition, a 550 nm PLE peak can be found when monitored at 650 nm, suggesting that the Si dangling bond (K^0) center is related to the excitation process. Based on the resonance electron transfer mechanism [21], a possible PL process is that photogeneration of carriers takes place in the Si dangling bond (K^0), while radiative recombination occurs in the quantum confined Si nanodots. Thus, resonant electron transfer from the Si K^0 center to conduction band of the quantum confined Si nanodots can contribute to the red light emission. Consequently, it can be inferred that the dominant EL band stems from band-to-band radiative recombination in the Si nanodots where quantum confinement effect plays a crucial role in the light emission.

Figure 4 shows the J-V curve obtained from the corresponding device. To explain the charge transport behavior, different conduction models, such as Fowler–Nordheim tunneling (FN), Poole–Frenkel emission (PF), and space charge-limited conduction (SCLC), are usually adopted for Si-based materials [13–14]. In this case, all the experimental data can be fitted well by $J = CE \exp\{-q[\psi_B - (qE/\pi\epsilon)^{0.5}]/\kappa T\}$, where C, ψ_B, and ϵ are the system-specific constant barrier height for electrons to escape from the traps and dielectric constant of the film, respectively. This relationship is well known as the PF emission [14], indicating that the carrier transport process is governed by PF emission. The inset in Fig. 3 reveals a linear relationship between the integrated EL intensity and injected current, implying that the white EL arises mainly from bipolar recombination of electron–hole pairs at the luminescent centers in which the a-Si nanodots are responsible for the red light emission while the radiative Si dangling bond (K^0) centers in the silicon nitride contribute to the 550 nm yellow emission.

In summary, strong white EL is observed at a low operating voltage from SiN-based devices containing Si nanodots with a density of over $4.6 \times 10^{12}/\text{cm}^2$. The white EL can be decomposed into two components, a strong red one and a weak yellow one. According to the PL characteristics, the red emission can be attributed to bipolar recombination of electron–hole pairs in the dense Si nanodots where quantum confinement plays a decisive role in the light emission. The weak yellow emission arises from the radiative Si dangling bond (K^0) center in the silicon nitride matrix.

This work is supported by the National Natural Science Foundation of China (NSFC; grants 60806046 and 60976063), Natural Science Foundation of Guangdong Province (S2011010001853), and Foundation for Distinguished Young Talents in Higher Education of Guangdong (LYM09101 and LYM10099). Partial support was also from the Basic Research Program of China under grant 2011CB922102, and Hong Kong Research Grants Council (RGC) General Research Funds (GRF) CityU 112510.

References

1. K. Chen, X. Huang, J. Xu, and D. Feng, Appl. Phys. Lett. **61**, 2069 (1992).
2. L. Pavesi, L. Dal Negro, C. Mazzoleni, G. Franzò, and F. Priolo, Nature **408**, 440 (2000).
3. W. L. Wu, J. Y. Fan, T. Qiu, X. Yang, G. G. Siu, and Paul K. Chu, Phys. Rev. Lett. **94**, 026102 (2005).
4. B.-H. Kim, C.-H. Cho, J.-S. Mun, M.-K. Kwon, T.-Y. Park, J. S. Kim, C. C. Byeon, J. Lee, and S.-J. Park, Adv. Mater. **20**, 3100 (2008).
5. N.-M. Park, C.-J. Choi, T.-Y. Seong, and S.-J. Park, Phys. Rev. Lett. **86**, 1355 (2001).
6. R. J. Walters, J. Kalkman, A. Polman, H. A. Atwater, and M. J. A. de Dood, Phys. Rev. B **73**, 132302 (2006).
7. C. Liu, C. Li, A. Ji, L. Ma, Y. Q. Wang, and Z. X. Cao, Appl. Phys. Lett. **86**, 223111 (2005).
8. M. V. Wolkin, J. Jorne, P. M. Fauchet, G. Allan, and C. Delerue, Phys. Rev. Lett. **82**, 197 (1999).
9. J. Zhou, G. R. Chen, Y. Liu, J. Xu, T. Wang, N. Wan, Z. Y. Ma, W. Li, C. Song, and K. J. Chen, Opt. Express **17**, 156 (2009).
10. G. R. Lin, C. J. Lin, and C. K. Lin, Opt. Express **15**, 2555 (2007).
11. B. M. Monroy, O. Crégut, M. Gallart, B. Hönerlage, and P. Gilliot, Appl. Phys. Lett. **98**, 261108 (2011).
12. L.-Y. Chen, W.-H. Chen, and F. C.-N. Hong, Appl. Phys. Lett. **86**, 193506 (2005).
13. R. Huang, H. Dong, D. Wang, K. Chen, X. Wang, J. Xu, and Z. Ma, Appl. Phys. Lett. **92**, 181106 (2008).
14. J. Warga, R. Li, S. N. Basu, and L. Dal Negro, Appl. Phys. Lett. **93**, 151116 (2008).
15. Z. H. Cen, T. P. Chen, L. Ding, Y. Liu, J. I. Wong, M. Yang, Z. Liu, W. P. Goh, F. R. Zhu, and S. Fung, Appl. Phys. Lett. **94**, 041102 (2009).
16. M. Wang, J. Huang, Z. Yuan, A. Anopchenko, D. Li, D. Yang, and L. Pavesi, J. Appl. Phys. **104**, 083505 (2008).
17. K. Murayama, K. Monji, and H. Deki, Phys. Status Solidi C, **7**, 674 (2010).
18. G.-R. Lin, Y.-H. Pai, C.-T. Lin, and C.-C. Chen, Appl. Phys. Lett. **96**, 263514 (2010).
19. J. Roberson and M. J. Powell, Appl. Phys. Lett. **44**, 415 (1984).
20. X. Wen, L. V. Dao, and P. Hannaford, J. Phys. D **40**, 3573 (2007).
21. X. L. Wu, T. Qiu, D. S. Hu, G. S. Huang, R. K. Yuan, G. G. Siu, and P. K. Chu, J. Chem. Phys. **125**, 054713 (2006).